

## Scattering of flexural wave in thin plate with multiple holes by using the null-field integral equation method

Wei-Ming Lee<sup>1</sup>, Jeng-Tzong Chen<sup>2</sup>, Ching-Lun Chien<sup>1</sup>, Yung-Cheng Wang<sup>1</sup>

<sup>1</sup> Department of Mechanical Engineering, China Institute of Technology, Taipei, Taiwan

<sup>2</sup> Department of Harbor and River Engineering, National Taiwan Ocean University, Keelung, Taiwan

E-mail:wmlee@cc.chit.edu.tw jtchen@mail.ntou.edu.tw

### Abstract

In this paper, a semi-analytical approach is proposed to solve the scattering problem of flexural waves and dynamic moment concentration factors in an infinite thin plate with multiple circular holes by using the null-field integral formulation in conjunction with degenerate kernels and Fourier series. In the proposed approach, all the kernels in the direct formulation are expanded into degenerate forms. By uniformly collocating points on the real boundary, a linear algebraic system is constructed. The scattering problem can be solved by decomposing it into two parts: incident wave field and radiation field. The radiation field is solved by using the proposed method and then the total field is obtained by adding it with the incident wave field. The results of dynamic moment concentration factors for the plate with one hole are compared with the analytical solution to verify the validity of the proposed method. For the cases of small wave number, the quasi-static results of a plate with one or multiple circular holes are compared with the static data of finite element method (FEM) using ABAQUS. The effect of distance between the centers of holes on dynamic moment concentration factors is also investigated by using the proposed method.

**Keywords:** scattering, flexural wave, dynamic moment concentration, biHelmholtz equation, null-field boundary integral equation, degenerate kernel, Fourier series

### 1. Introduction

Thin plates with multiple circular holes are widely used in engineering structures, e.g. missiles, aircraft, etc., either to reduce the weight of the whole structure or to increase the range of inspection. Geometric

discontinuities due to these holes result in the stress concentration, which reduce the load carrying capacity. The deformation and corresponding stresses produced by the dynamic force are propagated through the structure in the form of waves. At the irregular interface of different media, stress wave reflects in all directions, which is the phenomenon of scattering. It turns out that the scattering of the stress wave results in the dynamic stress concentration [1].

Nishimura and Jimbo [2] were two of the early investigators for the analytical study of the dynamic stress concentration. Pao [3] studied the scattering of flexural waves and dynamic stress concentrations around a circular hole, and proposed an analytical solution. Since then, most research work has focused on the scattering of elastic wave and dynamic stress concentration and has led to a rapid development of analytical or numerical approach such as the method of wave function expansion, complex variable method, boundary integral equation method (BIEM) and boundary element method (BEM) [1].

Kung [4] studied dynamic stress concentrations resulting from the scattering of flexural waves on the thin plate with one circular hole and gave the calculations of moment and shear forces as a function of frequency. Liu *et al.* [5] extended the complex variable function approach for statics to the case of dynamic loading. The complex variable function approach and conformal mapping technique were employed to solve diffraction problem of flexural waves by two cutouts [6] and dynamic concentration factors of plates with two circular holes were presented. Vernon *et al.* [7] applied the wave function expansion method to study the scattering properties of a single coated cylindrical anomaly located in a thin plate on which flexural waves propagate. Hayir *et al.* [8] applied

the image method to analyze the scattering and dynamic stress concentrations of elastic waves in plates with a circular hole subject to plane harmonic SH wave. Gao *et al.* [9] studied the scattering of flexural waves and calculated the dynamic stress concentration in the thin plate with the cutout by using the dual reciprocity boundary element method. Hu *et al.* [10] applied the image method and the wave function expansion method to study the multiple scattering of flexural waves in semi-infinite plates with a circular cutout. Recently, one monograph is devoted to discussing the multiple scattering in acoustics, electromagnetism, seismology and hydrodynamics [11].

From literature reviews stated previously, few papers except [6] have been published to date reporting the scattering of flexural wave in plate with more than one cutout. Furthermore, as Kobayashi and Nishimura [12] pointed out that the integral equation method seems to be most effective for two-dimensional steady-state flexural wave. In the paper, the boundary integral method is devoted to solving the multiple scattering of flexural wave and dynamic stress concentrations in plate with multiple circular holes.

It is noted that improper integrals on the boundary should be handled particularly when the BEM or BIEM is used. In the past, many researchers proposed several regularization techniques to deal with the singularity and hypersingularity [13]. In this paper, instead of using the previous concepts, the kernel function is recast into the degenerate kernel which is expanded into a series form on each side (interior and exterior) of the boundary by employing the addition theorem. Therefore, degenerate kernel, namely separable kernel, is a vital tool to study the perforated plate. Based on the direct boundary integral formulation, Chen *et al.* [14-16] recently proposed null-field integral equations in conjunction with degenerate kernels and Fourier series to solve boundary value problems with circular boundaries.

This paper presents a semi-analytical approach to solve scattering of flexural waves and dynamic moment concentration factors in a thin plate with multiple circular holes. A linear algebraic system will be constructed by taking finite terms of Fourier series after uniformly collocating points on the boundary. After determining the Fourier coefficients of unknown

boundary density, the displacement and corresponding section force produced by the incident flexural wave are determined by using the boundary integral equations for the domain point. For the plate problem, the slope (bending angle) and moment in the normal and tangential directions for the multiply-connected domain problem are determined with care under the adaptive observer system. Therefore, the operator of transformation matrix for the slope and moment is adopted to deal with this problem. Finally, the obtained result for an infinite plate with one circular hole is compared with the analytical solution [4] to verify the validity of the present method. For the cases of small wave number, the results for more than one hole will be compared with those of FEM using ABAQUS [17] to demonstrate the generality of the proposed method. Finally, the effect of central distance between holes on dynamic moment concentration factors is also investigated efficiently by the proposed method.

## 2. Problem statement and boundary integral formulation

### 2.1 Problem statement

The governing equation of the flexural wave for a uniform thin plate with randomly distributed circular holes as shown in Figure 1 is written as follows:

$$\nabla^4 u(x) = k^4 u(x), \quad x \in \Omega \quad (1)$$

where  $u$  is the out-of-plane elastic displacement,  $k^4 = \omega^2 \rho_0 h/D$ ,  $k(2\pi/\text{wave length})$  is the wave number of elastic wave,  $\omega$  is the circular frequency,  $\rho_0$  is the volume density,  $D = Eh^3/12(1-\nu^2)$  is the flexural rigidity,  $E$  denotes the Young's modulus,  $\nu$  is the Poisson ratio,  $h$  is the plate thickness and  $\Omega$  is the domain of the thin plate.

### 2.2 Boundary integral equation for the collocation point in the domain

The integral representation for the plate problem can be derived from the Rayleigh-Green identity [18] as follows:

$$u(x) = \int_B U(s,x)v(s)dB(s) - \int_B \Theta(s,x)m(s)dB(s) + \int_B M(s,x)\theta(s)dB(s) - \int_B V(s,x)u(s)dB(s) \quad (2)$$

$$\theta(x) = \int_B U_\theta(s,x)v(s)dB(s) - \int_B \Theta_\theta(s,x)m(s)dB(s) + \int_B M_\theta(s,x)\theta(s)dB(s) - \int_B V_\theta(s,x)u(s)dB(s) \quad (3)$$

$$m(x) = \int_B U_m(s,x)v(s)dB(s) - \int_B \Theta_m(s,x)m(s)dB(s) + \int_B M_m(s,x)\theta(s)dB(s) - \int_B V_m(s,x)u(s)dB(s) \quad (4)$$

$$v(x) = \int_B U_v(s,x)v(s)dB(s) - \int_B \Theta_v(s,x)m(s)dB(s) + \int_B M_v(s,x)\theta(s)dB(s) - \int_B V_v(s,x)u(s)dB(s) \quad (5)$$

$x \in \Omega$

where  $B$  is the boundary of the domain  $\Omega$ ,  $u(x)$ ,  $\theta(x)$ ,  $m(x)$  and  $v(x)$  are the displacement, slope, moment and shear force.  $s$  and  $x$  mean the source and field points, respectively. The kernel functions  $U(s,x)$ ,  $\Theta(s,x)$ ,  $M(s,x)$ ,  $V(s,x)$ ,  $U_\theta(s,x)$ ,  $\Theta_\theta(s,x)$ ,  $M_\theta(s,x)$ ,  $V_\theta(s,x)$ ,  $U_m(s,x)$ ,  $\Theta_m(s,x)$ ,  $M_m(s,x)$ ,  $V_m(s,x)$ ,  $U_v(s,x)$ ,  $\Theta_v(s,x)$ ,  $M_v(s,x)$  and  $V_v(s,x)$  in Eqs.(2)-(5) can be expanded to degenerate kernels by separating the source and field points and will be elaborated on later. The kernel function  $U(s,x)$  in Eq.(2) is the fundamental solution which satisfies

$$\nabla^4 U(s,x) - k^4 U(s,x) = \delta(s-x) \quad (6)$$

where  $\nabla^4$  is the biharmonic operator and  $\delta(s-x)$  is the Dirac-delta function, respectively. The fundamental solution is

$$U(s,x) = \frac{1}{8k^2} \left[ Y_0(kr) + iJ_0(kr) + \frac{2}{\pi} K_0(kr) \right], \quad (7)$$

where  $r \equiv |s-x|$  and  $i^2 = -1$ . The other three kernels  $\Theta(s,x)$ ,  $M(s,x)$  and  $V(s,x)$  in Eq.(2) can be obtained by applying the following slope, moment and effective shear operators defined by

$$K_\theta = \frac{\partial(\cdot)}{\partial n} \quad (8)$$

$$K_M = -D \left[ \nu \nabla^2(\cdot) + (1-\nu) \frac{\partial^2(\cdot)}{\partial n^2} \right] \quad (9)$$

$$K_V = -D \left[ \frac{\partial}{\partial n} \nabla^2(\cdot) + (1-\nu) \frac{\partial}{\partial t} \left( \frac{\partial}{\partial n} \left( \frac{\partial}{\partial t}(\cdot) \right) \right) \right] \quad (10)$$

to the kernel  $U(s,x)$  with respect to the source point, where  $\partial/\partial n$  and  $\partial/\partial t$  are the normal and tangential derivatives, respectively,  $\nabla^2$  means the Laplacian operator. In the polar coordinate of  $(R,\theta)$ , the three kernel functions can be rewritten as:

$$\Theta(s,x) = K_{\theta,s}(U(s,x)) = \frac{\partial U(s,x)}{\partial R} \quad (11)$$

$$M(s,x) = K_{M,s}(U(s,x)) = -D \left[ \nu \nabla^2 U(s,x) + (1-\nu) \frac{\partial^2 U(s,x)}{\partial R^2} \right] \quad (12)$$

$$V(s,x) = K_{V,s}(U(s,x)) = -D \left[ \frac{\partial}{\partial R} \left( \nabla_s^2 U(s,x) \right) + (1-\nu) \left( \frac{1}{R} \right) \frac{\partial}{\partial \theta} \left( \frac{\partial}{\partial R} \left( \frac{1}{R} \frac{\partial U(s,x)}{\partial \theta} \right) \right) \right] \quad (13)$$

The expressions for  $\theta(x)$ ,  $m(x)$  and  $v(x)$  in

Eqs.(3)-(5), obtained by applying the operators in Eqs.(8)-(10) to  $u(x)$  in Eq. (2) with respect to the field point  $x(\rho,\phi)$ , are

$$\theta(x) = K_{\theta,x}(u(x)) = \frac{\partial u(x)}{\partial \rho}, \quad (14)$$

$$m(x) = K_{M,x}(u(x)) = -D \left[ \nu \nabla^2 u(x) + (1-\nu) \frac{\partial^2 u(x)}{\partial \rho^2} \right], \quad (15)$$

$$v(x) = K_{V,x}(u(x)) = -D \left[ \frac{\partial}{\partial \rho} \left( \nabla_s^2 u(x) \right) + (1-\nu) \left( \frac{1}{\rho} \right) \frac{\partial}{\partial \phi} \left( \frac{\partial}{\partial \rho} \left( \frac{1}{\rho} \frac{\partial u(x)}{\partial \phi} \right) \right) \right] \quad (16)$$

By the same way, the kernel functions  $U_\theta(s,x)$ ,  $\Theta_\theta(s,x)$ ,  $M_\theta(s,x)$ ,  $V_\theta(s,x)$ ,  $U_m(s,x)$ ,  $\Theta_m(s,x)$ ,  $M_m(s,x)$ ,  $V_m(s,x)$ ,  $U_v(s,x)$ ,  $\Theta_v(s,x)$ ,  $M_v(s,x)$  and  $V_v(s,x)$  can be obtained by applying the operators in Eqs.(8)-(10) respectively to the kernel functions  $U$ ,  $\Theta$ ,  $M$  and  $V$  with respect to the field point  $x(\rho,\phi)$ .

### 2.3 Null-field integral equations

The null-field integral equations derived by collocating the field point outside the domain (including the boundary point if exterior degenerate kernels are adopted) are shown as follows:

$$0 = \int_B U(s,x)v(s)dB(s) - \int_B \Theta(s,x)m(s)dB(s) + \int_B M(s,x)\theta(s)dB(s) - \int_B V(s,x)u(s)dB(s) \quad (17)$$

$$0 = \int_B U_\theta(s,x)v(s)dB(s) - \int_B \Theta_\theta(s,x)m(s)dB(s) + \int_B M_\theta(s,x)\theta(s)dB(s) - \int_B V_\theta(s,x)u(s)dB(s) \quad (18)$$

$$0 = \int_B U_m(s,x)v(s)dB(s) - \int_B \Theta_m(s,x)m(s)dB(s) + \int_B M_m(s,x)\theta(s)dB(s) - \int_B V_m(s,x)u(s)dB(s) \quad (19)$$

$$0 = \int_B U_v(s,x)v(s)dB(s) - \int_B \Theta_v(s,x)m(s)dB(s) + \int_B M_v(s,x)\theta(s)dB(s) - \int_B V_v(s,x)u(s)dB(s), \quad (20)$$

$$x \in \Omega^C \cup B,$$

where  $\Omega^C$  is the complementary domain of  $\Omega$ . Once kernel functions are expressed in proper degenerate forms, which will be described in the next subsection, the collocation points can be exactly located on the real boundary, that is  $x \in \Omega^C \cup B$ . Since the four equations of Eqs.(17)-(20) in the plate formulation are provided, there are 6 ( $C_2^4$ ) options for choosing any two equations to solve the problems. Kernels in Eq.(20) involve higher-order derivatives, which may decrease

both the convergence rate and computational efficiency. For the purpose of computational efficiency, Eqs. (17) and (18) are used to analyze the plate problem.

## 2.4 Degenerate kernels and Fourier series for boundary densities

In the polar coordinate, the field point and source point can be expressed as  $(\rho, \phi)$  and  $(R, \theta)$ , respectively. By employing the separation technique for the source and field points, the kernel functions  $U(s, x)$  are expanded in the series form as follows:

$$\begin{aligned} U^I(s, x) &= \frac{1}{8k^2} \sum_{m=0}^{\infty} \varepsilon_m \{J_m(k\rho)Y_m(kR) \\ &\quad + \frac{2}{\pi} I_m(\lambda\rho)K_m(kR)\} \cos[m(\theta - \phi)], \quad \rho < R \\ U^E(s, x) &= \frac{1}{8k^2} \sum_{m=0}^{\infty} \varepsilon_m \{J_m(kR)Y_m(k\rho) \\ &\quad + \frac{2}{\pi} I_m(kR)K_m(k\rho)\} \cos[m(\theta - \phi)], \quad \rho \geq R \end{aligned} \quad (21)$$

where  $\varepsilon_m$  is the Neumann factor ( $\varepsilon_m = 1, m=0$ ;  $\varepsilon_m = 2, m=1, 2, \dots, \infty$ ) and the superscripts "I" and "E" denote the interior and exterior cases for the degenerate kernel  $U(s, x)$  to distinguish  $\rho < R$  and  $\rho > R$ , respectively. The degenerate kernels  $\theta(s, x)$ ,  $M(s, x)$  and  $V(s, x)$  in the null-field boundary integral equations can be obtained by applying the operators of Eqs.(11)-(13) to the degenerate kernel  $U(s, x)$  of Eq.(21).

In order to fully utilize the geometry of circular boundary, the displacement  $u(s)$ , slope  $\theta(s)$ , moment  $m(s)$  and shear force  $v(s)$  along the circular boundaries in the null-field integral equations can be expanded in terms of Fourier series, respectively, as shown below:

$$u(s) = u_{c0} + \sum_{n=1}^M (u_{cn} \cos n\theta + u_{sn} \sin n\theta), \quad s \in B, \quad (22)$$

$$\theta(s) = \theta_{c0} + \sum_{n=1}^M (\theta_{cn} \cos n\theta + \theta_{sn} \sin n\theta), \quad s \in B, \quad (23)$$

$$m(s) = m_{c0} + \sum_{n=1}^M (m_{cn} \cos n\theta + m_{sn} \sin n\theta), \quad s \in B, \quad (24)$$

$$v(s) = v_{c0} + \sum_{n=1}^M (v_{cn} \cos n\theta + v_{sn} \sin n\theta), \quad s \in B, \quad (25)$$

where  $u_{c0}$ ,  $u_{cn}$ ,  $u_{sn}$ ,  $\theta_{c0}$ ,  $\theta_{cn}$ ,  $\theta_{sn}$ ,  $m_{c0}$ ,  $m_{cn}$ ,  $m_{sn}$ ,  $v_{c0}$ ,  $v_{cn}$  and  $v_{sn}$  are the Fourier coefficients and  $M$  is the number of Fourier series terms.

## 3 Adaptive observer system and transformation of tensor components

### 3.1 Adaptive observer system

Consider an infinite plate with circular holes as shown in Fig. 1. Since the direct boundary integral equations are frame indifferent (*i.e.* rule of objectivity), the origin of the observer system can be adaptively located on the center of the corresponding boundary contour under integration. Adaptive observer system is chosen to fully employ the circular property, which takes the full advantage of both Fourier series to represent boundary variables and degenerate-kernel expressions in the polar coordinate. Figure 2 shows the boundary integration for the circular boundaries in the adaptive observer system. The dummy variable in the circular contour integration is the angle ( $\theta$ ) instead of radial coordinate ( $R$ ). By using the adaptive system, all the boundary integrals can be determined analytically free of principal value senses.

### 3.2 Transformation of tensor components

Since the slope, moment and effective shear force are calculated in the plate problem, potential gradient or higher-order gradient needs to be manipulated with care. Special treatment for the potential gradient should be taken care as the source and field points locate on different circular boundaries. As shown in Figure 3, the angle  $\phi_i$  of the collocation point  $x_i$  is described in the center of the circle under integration and the angle  $\phi_c$  is described in the center of the circle on which collocation point is located. According to the transformation law for the components of tensor, we have

$$\begin{bmatrix} (\cdot)_n \\ (\cdot)_t \end{bmatrix} = \begin{bmatrix} \cos(\delta) & \sin(\delta) \\ -\sin(\delta) & \cos(\delta) \end{bmatrix} \begin{bmatrix} (\cdot)_r \\ (\cdot)_\theta \end{bmatrix}, \quad (26)$$

$$\begin{bmatrix} (\cdot)_{nn} \\ (\cdot)_{nt} \\ (\cdot)_{tt} \end{bmatrix} = \begin{bmatrix} \cos^2(\delta) & \sin^2(\delta) & 2\sin(\delta)\cos(\delta) \\ \sin^2(\delta) & \sin^2(\delta) & -2\sin(\delta)\cos(\delta) \\ -\sin(\delta)\cos(\delta) & \sin(\delta)\cos(\delta) & \cos^2(\delta) - \sin^2(\delta) \end{bmatrix} \begin{bmatrix} (\cdot)_{rr} \\ (\cdot)_{\theta\theta} \\ (\cdot)_{r\theta} \end{bmatrix}, \quad (27)$$

Based on Eqs. (26) and (27), the general rotated slope, normal bending and tangential bending moment kernels can be obtained by following operators:

$$K_\theta^R = \cos(\delta) \frac{\partial(\cdot)}{\partial n} + \sin(\delta) \frac{\partial(\cdot)}{\partial t} \quad (28)$$

$$\begin{aligned} K_N^R &= -D \left\{ [v + (1-v)\sin^2(\delta)] \nabla^2(\cdot) + \cos(2\delta)(1-v) \frac{\partial^2(\cdot)}{\partial n^2} \right. \\ &\quad \left. + \sin(2\delta)(1-v) \frac{\partial}{\partial n} \left\{ \frac{\partial(\cdot)}{\partial t} \right\} \right\} \end{aligned} \quad (29)$$

$$\begin{aligned} K_T^R &= -D \left\{ [v + (1-v)\cos^2(\delta)] \nabla^2(\cdot) + \cos(2\delta)(v-1) \frac{\partial^2(\cdot)}{\partial n^2} \right. \\ &\quad \left. - \sin(2\delta)(1-v) \frac{\partial}{\partial n} \left\{ \frac{\partial(\cdot)}{\partial t} \right\} \right\} \end{aligned} \quad (30)$$

where  $\delta = \phi_c - \phi_i$ . When the angle  $\phi_c$  equals to the angle  $\phi_i$  or the angle difference  $\delta$  equals to zero, Eqs.(28) and (29) are simplified to the Eqs.(14) and (15). Considering non-concentric cases, the degenerate kernels,  $U_\theta(s,x)$ ,  $\Theta_\theta(s,x)$ ,  $M_\theta(s,x)$ ,  $V_\theta(s,x)$ ,  $U_m(s,x)$ ,  $\Theta_m(s,x)$  and  $M_m(s,x)$  can be obtained by applying the operators of Eqs.(28)-(29) to the degenerate kernel  $U(s,x)$ ,  $\Theta(s,x)$ ,  $M(s,x)$  and  $V(s,x)$  with respect to the field point  $x$ .

#### 4 Linear algebraic system

Consider an infinite plate containing  $H$  nonoverlapping circular holes centered at the position vector  $\mathbf{o}_j$  ( $j=1, 2, \dots, H$ ), as shown in Fig. 2 in which  $R_j$  denotes the radius of the  $j$ th circular region,  $\mathbf{x}_j$  is the collocation point on the  $j$ th circular boundary and  $B_j$  is the boundary of the  $j$ th circular hole. By uniformly collocating  $N$  ( $=2M+1$ ) points on each circular boundary in Eqs. (17) and (18), we have

$$0 = \sum_{j=1}^H \int_{B_j} \{U(s,x)v(s) - \Theta(s,x)m(s) + M(s,x)\theta(s) - V(s,x)u(s)\} dB_j(s), \quad x \in B, \quad (31)$$

$$0 = \sum_{j=1}^H \int_{B_j} \{U_\theta(s,x)v(s) - \Theta_\theta(s,x)m(s) + M_\theta(s,x)\theta(s) - V_\theta(s,x)u(s)\} dB_j(s), \quad x \in B. \quad (32)$$

It must be noted that  $U$ ,  $\Theta$ ,  $M$ ,  $U_\theta$  and  $\Theta_\theta$  are weakly singular,  $V$  and  $M_\theta$  are singular and  $V_\theta$  is hypersingular [25] since we select the null-field point on the boundary in the real computation. The main gain by using the degenerate kernel in the BIE is that singular as well as hypersingular integrals due to the kernels can be transformed to the series sum free of facing principal values. The selection of interior or exterior degenerate kernel depends on  $\rho < R$  or  $\rho > R$ , respectively, according to the observer system. For the  $B_j$  circular boundary integrals, the degenerate kernels of  $U(s,x)$ ,  $\Theta(s,x)$ ,  $M(s,x)$ ,  $V(s,x)$ ,  $U_\theta(s,x)$ ,  $\Theta_\theta(s,x)$ ,  $M_\theta(s,x)$  and  $V_\theta(s,x)$  are utilized and boundary densities  $u(s)$ ,  $\theta(s)$ ,  $m(s)$  and  $v(s)$  along the circular boundary are substituted by using the Fourier series of Eqs.(22)-(25), respectively. In the  $B_j$  integration, the origin of the observer system is adaptively set to collocate at the center  $\mathbf{o}_j$  from which the degenerate kernels and Fourier series are described. By using orthogonal property, a linear

algebraic system can be written as follows:

$$\begin{bmatrix} U^{11} & -\Theta^{11} & U^{12} & -\Theta^{12} & \dots & U^{1H} & -\Theta^{1H} \\ U_\theta^{11} & -\Theta_\theta^{11} & U_\theta^{12} & -\Theta_\theta^{12} & \dots & U_\theta^{1H} & -\Theta_\theta^{1H} \\ U^{21} & -\Theta^{21} & U^{22} & -\Theta^{22} & \dots & U^{2H} & -\Theta^{2H} \\ U_\theta^{21} & -\Theta_\theta^{21} & U_\theta^{22} & -\Theta_\theta^{22} & \dots & U_\theta^{2H} & -\Theta_\theta^{2H} \\ \vdots & \vdots & \vdots & \vdots & \ddots & \vdots & \vdots \\ U^{H1} & -\Theta^{H1} & U^{H2} & -\Theta^{H2} & \dots & U^{HH} & -\Theta^{HH} \\ U_\theta^{H1} & -\Theta_\theta^{H1} & U_\theta^{H2} & -\Theta_\theta^{H2} & \dots & U_\theta^{HH} & -\Theta_\theta^{HH} \end{bmatrix} \begin{Bmatrix} v^1 \\ m^1 \\ v^2 \\ m^2 \\ \vdots \\ v^H \\ m^H \end{Bmatrix} = \begin{bmatrix} -M^{11} & V^{11} & -M^{12} & V^{12} & \dots & -M^{1H} & V^{1H} \\ -M_\theta^{11} & V_\theta^{11} & -M_\theta^{12} & V_\theta^{12} & \dots & -M_\theta^{1H} & V_\theta^{1H} \\ -M^{21} & V^{21} & -M^{22} & V^{22} & \dots & -M^{2H} & V^{2H} \\ -M_\theta^{21} & V_\theta^{21} & -M_\theta^{22} & V_\theta^{22} & \dots & -M_\theta^{2H} & V_\theta^{2H} \\ \vdots & \vdots & \vdots & \vdots & \ddots & \vdots & \vdots \\ -M^{H1} & V^{H1} & -M^{H2} & V^{H2} & \dots & -M^{HH} & V^{HH} \\ -M_\theta^{H1} & V_\theta^{H1} & -M_\theta^{H2} & V_\theta^{H2} & \dots & -M_\theta^{HH} & V_\theta^{HH} \end{bmatrix} \begin{Bmatrix} \theta^1 \\ u^1 \\ \theta^2 \\ u^2 \\ \vdots \\ \theta^H \\ u^H \end{Bmatrix} \quad (33)$$

where  $H$  denotes the number of circular boundaries. For brevity, a unified form  $[U^{ij}]$  ( $i=1,2,3,\dots,H$  and  $j=1,2,3,\dots,H$ ) denote the response of  $U(s,x)$  kernel on the  $i$ th circle due to the source on the  $j$ th circle. Otherwise, the same definition is for  $[\Theta^{ij}]$ ,  $[M^{ij}]$ ,  $[V^{ij}]$ ,  $[U_\theta^{ij}]$ ,  $[\Theta_\theta^{ij}]$ ,  $[M_\theta^{ij}]$  and  $[V_\theta^{ij}]$  kernels. The explicit expressions for sub-vectors  $[u^i]$ ,  $[\theta^i]$ ,  $[m^i]$  and  $[v^i]$  can be described as follows:

$$u^i = \begin{Bmatrix} u_{c0}^i \\ u_{c1}^i \\ \vdots \\ u_{s1}^i \\ \vdots \\ u_{cM}^i \\ \vdots \\ u_{sM}^i \end{Bmatrix}, \quad \theta^i = \begin{Bmatrix} \theta_{c0}^i \\ \theta_{c1}^i \\ \vdots \\ \theta_{s1}^i \\ \vdots \\ \theta_{cM}^i \\ \vdots \\ \theta_{sM}^i \end{Bmatrix}, \quad m^i = \begin{Bmatrix} m_{c0}^i \\ m_{c1}^i \\ \vdots \\ m_{s1}^i \\ \vdots \\ m_{cM}^i \\ \vdots \\ m_{sM}^i \end{Bmatrix}, \quad v^i = \begin{Bmatrix} v_{c0}^i \\ v_{c1}^i \\ \vdots \\ v_{s1}^i \\ \vdots \\ v_{cM}^i \\ \vdots \\ v_{sM}^i \end{Bmatrix}. \quad (34)$$

The explicit expressions for the sub-matrices of  $[U^{ij}]$ ,  $[\Theta^{ij}]$ ,  $[M^{ij}]$ ,  $[V^{ij}]$ ,  $[U_\theta^{ij}]$ ,  $[\Theta_\theta^{ij}]$ ,  $[M_\theta^{ij}]$  and  $[V_\theta^{ij}]$  can be written as shown below:

$$K^{ij} = \begin{bmatrix} K_{0c}^{ij}(\rho_1, \phi_1) & K_{1c}^{ij}(\rho_1, \phi_1) & K_{1s}^{ij}(\rho_1, \phi_1) & \dots & K_{Ms}^{ij}(\rho_1, \phi_1) \\ K_{0c}^{ij}(\rho_2, \phi_2) & K_{1c}^{ij}(\rho_2, \phi_2) & K_{1s}^{ij}(\rho_2, \phi_2) & \dots & K_{Ms}^{ij}(\rho_2, \phi_2) \\ \vdots & \vdots & \vdots & \ddots & \vdots \\ \vdots & \vdots & \vdots & \ddots & \vdots \\ K_{0c}^{ij}(\rho_N, \phi_N) & K_{1c}^{ij}(\rho_N, \phi_N) & K_{1s}^{ij}(\rho_N, \phi_N) & \dots & K_{Ms}^{ij}(\rho_N, \phi_N) \end{bmatrix}_{N \times N} \quad (35)$$

where  $K$  can be either one of  $U$ ,  $\Theta$ ,  $M$ ,  $V$ ,  $U_\theta$ ,  $\Theta_\theta$ ,  $M_\theta$  and  $V_\theta$ . The notations  $\phi_k$  and  $\rho_k$  ( $k=1,2,3,\dots,N$ ) shown in Fig. 3 are the angle and radius of the  $k$ -th collocation point on the  $i$ -th circular boundary with respect to the center of the  $j$ -th circular boundary (the origin of the observer system) and the element of the sub-matrices can be determined by

$$K_{nc}^{ij}(\rho_k, \phi_k) = \int_0^{2\pi} K(R_j, \theta_j; \rho_k, \phi_k) \cos(n\theta_j) (R_j d\theta_j), \quad n=0,1,2,\dots,M, \quad (36)$$

$$K_{ns}^{ij}(\rho_k, \phi_k) = \int_0^{2\pi} K(R_j, \theta_j; \rho_k, \phi_k) \sin(n\theta_j) (R_j d\theta_j), \quad n=1,2,\dots,M \quad (37)$$

in which the selection of interior or exterior degenerate kernel depends on the position of collocation point with

respective to the center of circle under integration as shown in Fig. 3

## 5 Dynamic moment concentration factor and techniques for solving scattering problems

Considering an infinite thin plate with multiple holes subject to incident flexural wave, the boundary conditions of the hole are free. For this scattering problem, it can be decomposed into two parts, (a) incident wave field and (b) radiation field, as shown in Fig. 4. For matching the boundary condition, the radiation boundary condition in part (b) is obtained as the minus quantity of incident wave function, e.g.  $m^R = -m^I; v^R = -v^I$  for the free edge where the superscripts  $R$  and  $I$  denote radiation and incidence, respectively. By substituting the known radiation boundary conditions,  $-m^I$  and  $-v^I$ , into the left hand side of Eq. (33), the unknown boundary data,  $u$  and  $\theta$ , can be solved. After calculating the displacement, slope, moment and effective shear force along the boundary, the radiation field can be solved by employing the boundary integral equation for the domain point of Eqs. (2)-(5). The scattering field is determined by superimposing radiation field and incident field. The tangential bending moment  $M_t$  can be determined by applying the operator in Eq.(30) to Eq.(2) with respective to the field point.

An incident flexural wave is represented by

$$u_0^{(i)} e^{ik(x \cos(\phi_0) + y \sin(\phi_0))} \quad (38)$$

where  $u_0^{(i)}$  is the amplitude of incident wave,  $k$  is the wave number and  $\phi_0$  is the incident angle. Under the polar coordinate, the bending moment and effective shear force induced by the incident wave can be determined by substituting Eq. (38) into Eqs.(9) and (10). By setting the amplitude of incident wave  $u_0^{(i)} = 1$ , the amplitude of moment produced by the incident wave is

$$M_0 = Dk^2 \quad (39)$$

The dynamic moment concentration factor (DMCF) can be determined as

$$DMCF = M_t / M_0 \quad (40)$$

## 6 Numerical results and discussions

Scattering problems of flexural wave in thin plate

with multiple holes are solved and dynamic moment concentration factors are determined by using the present method. For the cases of small wave number, the same plate problem is independently conducted by using FEM (the ABAQUS software) for comparison. In all cases, the inner boundary is subject to the free boundary condition and the thickness of plate is 0.002m.

### Case 1: An infinite plate with one hole [1,4,9]

An infinite plate with one hole (radius  $a = 1m$ ) subject to the incident flexural wave with  $\phi_0 = 0$  and different wave number is considered as shown in Figure 5. Figure 6 shows the DMCF on the circular boundary, at  $\pi/2$ , versus the dimensionless wave number by using different number of terms of Fourier series. From the convergence analysis, the required number of Fourier series of the present method to approach the analytic solution increases as the wave number of incident wave becomes large. Results of the present method match well those of analytic method when the number of terms of Fourier series amounts to  $M = 10$ .

In the limit of zero wave number [1] like  $k = 0.005$ , the incident excitation is similar to the application of static moment  $M_{xx} = M_0$  and  $M_{yy} = \nu M_0$  at the four sides of a plate. Accordingly, a  $16m \times 16m$  plate with one hole subject to static bending moments,  $M_{xx} = 1.0$  and  $M_{yy} = 0.3$  at the four sides is considered. The FEM model with 25567 triangle elements is shown in Figure 7(a) and the result of the normalized tangential bending moment around the hole is shown in Figure 7(b). By using the present method, the unknown boundary densities of the plate are expressed in terms of Fourier series and the numerical result of DMCF around the hole using fewer bases of Fourier series terms ( $M = 10$ ) is shown in Figure 7(c). The analytical solution [1] is also shown in Figure 7(d) and good agreements are made after comparing with three approaches, the present method, analytical solution and FEM.

Figure 8 shows that the real and imaginary parts of DMCF on the circular boundary at  $\pi/2$  versus the dimensionless wave number for various Poisson ratios by using the present method and analytical solution [1]. It indicates that both results match well and DMCF depends on the Poisson ratio of the plate as well as the incident wave number. The real and imaginary parts of

DMCF along the circular boundary are shown in Figure 9, which agree with the results reported in [10].

#### Case 2: An infinite plate with two holes [6]

An infinite plate with two holes (radius  $a = 1m$ ) subject to the incident flexural wave with  $\phi_0 = 0$  and different wave number is considered as shown in Figure 10, where  $L$  is the central distance of two holes. For the case of  $L = 2.1m$ , Figure 11 shows the DMCF on the upper circular boundary, at  $-\pi/2$ , versus the dimensionless wave number by using different number of terms of Fourier series. From the convergence analysis, the results using fewer terms of Fourier series show some peaks due to the close distance of two holes. Even so, the convergence is fast achieved when the number of Fourier series  $M$  reaches twenty.

After comparing with the proposed method, we consider a  $16m \times 22m$  plate with two holes ( $L = 2.1m$ ) subject to static bending moments,  $M_{xx} = 1.0$  and  $M_{yy} = 0.3$  at the four sides. The FEM model with 49024 triangle elements is shown in Figure 12(a) and the result of the normalized tangential bending moment around the hole is shown in Figure 12(b). The result of the present method for  $k = 0.005$  is shown in Figure 12(c) and good agreements are made after comparison.

The distribution of the amplitude of DMCF on the circular boundary, solid line for one hole and dash line for the upper one of two holes, are shown in Figure 13. Figure 14 shows the DMCF at the upper circular edge ( $-\pi/2$ ) versus the dimensionless central distance under different incident wave number, where the dot line denotes the result of one hole. It indicates that when the central distance between two holes gradually increases, the results for the case of two holes will approach that of one hole. The results show regular phenomenon and the period is  $2\pi/k$  which can not be found in [6]. Finally, the ineffective distance  $L_m$  is defined as the central distance required for the dynamic moment concentration factor of two holes to decrease and stay within two percentage of that of one hole. Numerical result indicates that the ineffective distance initially increase and then decrease as wave number increase.

### 7 Concluding remarks

A semi-analytical approach to solve the scattering problem of flexural waves and to determine dynamic moment concentration factors in an infinite thin plate

with multiple circular holes was proposed. The scattering problem can be treated by decomposing it into two parts: incident wave field and radiation field. The radiation field was determined by employing the null-field integral formulation in conjunction with degenerate kernels, tensor transformation and Fourier series. All the improper integrals in the null-field integral formulation were avoided by using the degenerate kernels and were easily calculated through the series sum. For the general exterior case, the rotated degenerate kernels have been derived in the adaptive observer system. Once the Fourier coefficients of boundary densities have been determined, the flexural wave scattering field and dynamic moment concentrations can be obtained by using the boundary integral equations for domain points in conjunction with general rotated degenerate kernels. For an infinite plate with one hole, good agreement between the results of the present method and those of analytical solution is observed. For the cases of small wave number, the present results for a plate with one or multiple circular holes are compared with the static case of finite element method (FEM) using ABAQUS. Convergence rate depends on two parameters of the incident wave number and the central distance between two holes. Test of convergence was done in our numerical results. The effect of the central distance on DMCF has been studied by using the present method. As can be seen from the numerical results, the present method provides a semi-analytic solution for the dynamic moment concentration factors in infinite thin plates with multiple circular holes subject to the incident flexural wave, since its analytical solution is not yet available.

### References

- [1] Pao, Y. H., Mow, C.C., 1972. Diffraction of elastic waves and dynamics stress concentration. Crane, New York.
- [2] Nishimura, G., Jimbo, Y., 1955. A dynamical problem of stress concentration. Journal of the Faculty of Engineering, University of Tokyo, Japan, 24, 101.
- [3] Pao, Y.H., 1962. Dynamical stress concentration in an elastic plate. Transactions of the ASME Journal of Applied Mechanics June, 299-305.
- [4] Kung, George C. S., 1964. Dynamical stress

concentration in an elastic plate. M.S. Thesis, Cornell University, Ithaca, NY.

[5] Lin, D., Gai, B., Tao, G., 1982. Applications of the method of complex functions to dynamic stress concentrations. *Wave Motion* 4, 293-304.

[6] Hu, C., Ma, X. R., Huang, W. H., 1998. Dynamic stress concentrations in thin plates with two circular cutouts. *Acta Mechanica Sinica* 30, 5, 587-596.

[7] Norris, A. N., Vemula, C., 1995. Scattering of flexural waves on thin plates. *Journal of Sound and Vibration* 181, 115-125.

[8] Hayir, A., Bakirtas, I., 2004. A note on plate having a circular cavity excited by plane harmonic SH waves. *Journal of Sound and Vibration* 271, 241-255.

[9] Gao, S. W., Wang, Y. S., Zhang, Z. M., Ma, R. X., 2005. Dual reciprocity boundary element method for flexural waves in thin plate with cutout. *Applied Mathematics and Mechanics* 26, 12, 1564-1573.

[10] Hu, C., Fang, X., Huang, W., 2007. Multiple scattering of flexural waves in a semi-infinite thin plate with a cutout. *International Journal of Solids and Structures* 44, 436-446.

[11] Martin, P.A., 2006. Multiple scattering interaction of time-harmonic wave with N obstacles. Cambridge University Press, UK.

[12] Kobayashi, S., Nishimura, N., 1981. Transient Stress Analysis of Tunnels and Caverns of Arbitrary Shape Due to Traveling Waves. in: *Developments in Boundary Element Methods-II*, Banerjee, P. K., and Shaw, R. P., eds., Applied Science, London, 177-210.

[13] Chen J. T., Hong H. K., 1999. Review of dual boundary element methods with emphasis on hypersingular integrals and divergent series. *Applied Mechanics Reviews ASME* 52, 1, 17-33.

[14] Chen J.T., Shen, W. C., Wu, A.C., 2006. Null-field integral equations for stress field around circular holes under anti-plane shear. *Eng Ana Bound Elem* 30, 205-217.

[15] Chen, J.T., Hsiao, C. C., Leu, S. Y., 2006. Null-field integral equation approach for plate problems with circular holes. *Transactions of the ASME Journal of Applied Mechanics* 73, 679-693.

[16] Chen, J.T., Shen, W. C., Chen, P. Y., 2006. Analysis of circular torsion bar with circular holes using null-field approach. *Computer Modeling in Engineering Science* 12, 2, 109-119.

[17] ABAQUS 6.5 2004. Hibbitt, Karlsson and Sorensen, Inc. RI.

[18] Kitahara, M., 1985. *Boundary Integral Equation Methods in Eigenvalue Problems of Elastodynamics and Thin Plates*. Elsevier: Amsterdam.

[19] Hutchinson, J. R., 1991. Analysis of plates and shells by boundary collocation. In: Beskos DE (ed) *Boundary Elements Analysis of Plates and Shells*. Springer Berlin, 314-368.

[20] Chen, J. T., Chen, C. T., Chen, P. Y., Chen, I. L. 2007. A semi-analytical approach for radiation and scattering problems with circular boundaries. *Computer Methods in Applied Mechanics and Engineering* 196, 2751-2764.

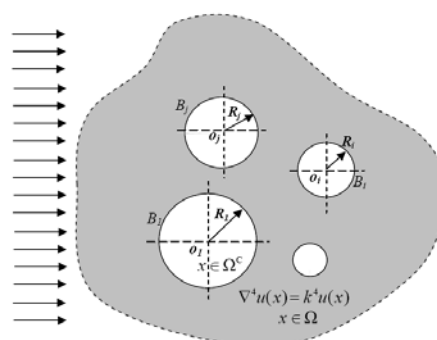


Figure 1 Problem statement for an infinite plate with multiple circular holes subject to an incident flexural wave

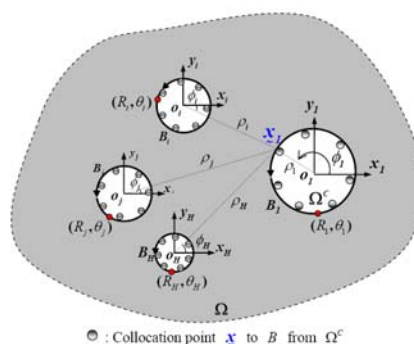


Figure 2 Collocation point and boundary contour integration in the boundary integral equation by using the adaptive observer system

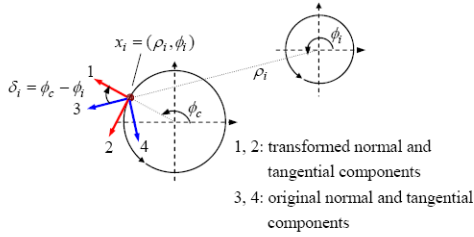
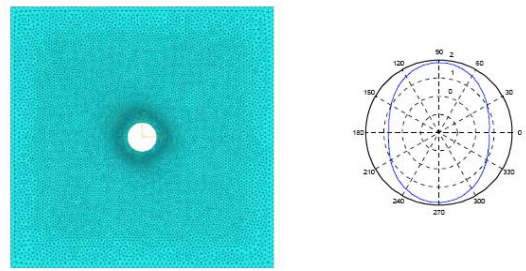


Figure 3 Transformation of tensor components



(a) Finite element mesh using ABAQUS (b) FEM (ABAQUS, under equivalent static loading)

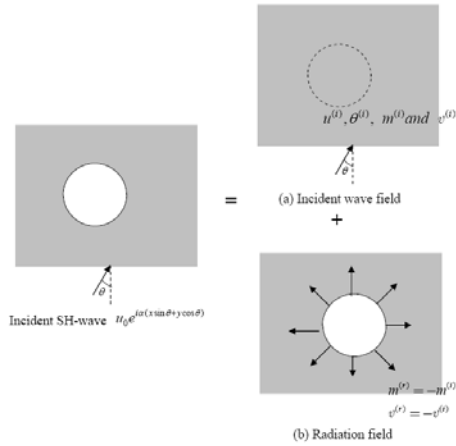


Figure 4 The decomposition of scattering problem into (a) incident wave field and (b) radiation field

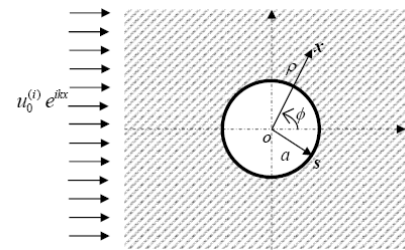


Figure 5 An infinite plate with one hole subject to an incident flexural wave

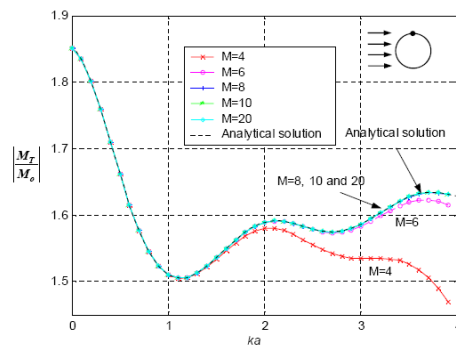
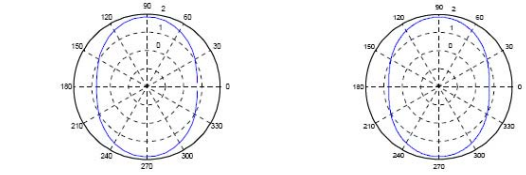


Figure 6 Dynamic moment concentration factor on the circular boundary ( $\theta = \pi / 2$ ) versus the dimensionless wave number by using different number of terms of Fourier series



(c) Present method ( $M=10, ka=0.005$ ) (d) Analytical solution ( $ka=0.005$ )

Figure 7 Distribution of dynamic moment concentration factors on the circular boundary by using different methods, the present method, analytical solution and FEM

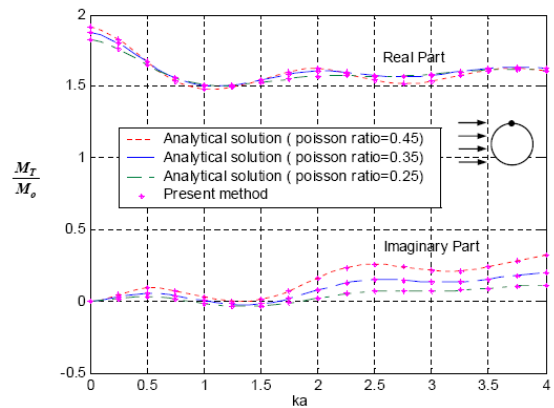


Figure 8 The real and imaginary parts of DMCF on the circular boundary ( $\theta = \pi / 2$ ) versus the dimensionless wave number for various Poisson ratios

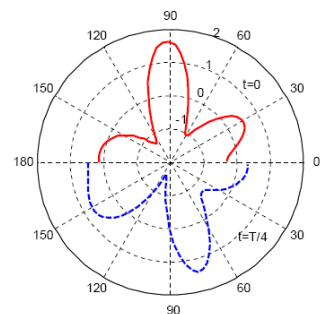


Figure 9 Distribution of DMCF ( $M_T / M_0$ ) on the circular boundary, solid line (real part) for  $t = 0$  for, dash line (imaginary part) for  $t = T/4$  ( $ka = 5.0$ )

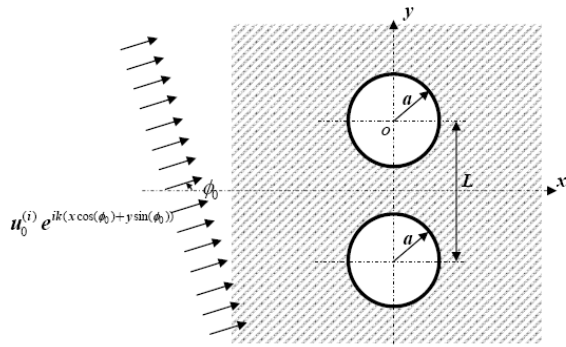


Figure 10 An infinite plate with two holes subject to an incident flexural wave with an incident angle  $\phi_0$

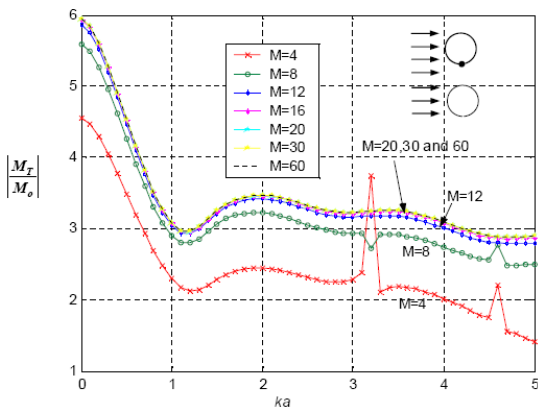


Figure 11 DMCF on the upper circular boundary ( $\theta = -\pi/2$ ) versus the dimensionless wave number by using different number of terms of Fourier series ( $L/a = 2.1$ )

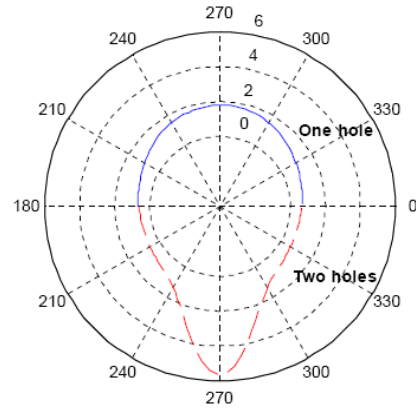


Figure 13. Distribution of DMCF ( $M_T / M_0$ ) on the circular boundary, solid line for one hole and dash line for the upper one of two holes ( $L=2.1a, ka = 0.2$ )

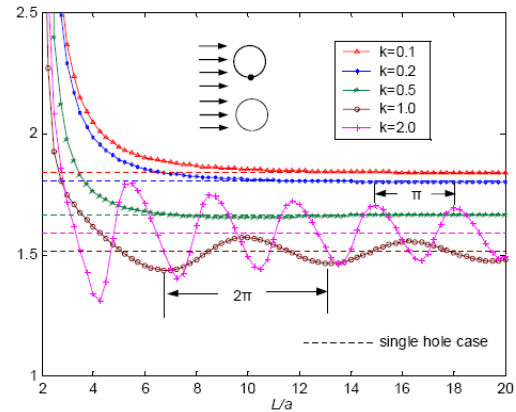


Figure 14. DMSF ( $M_\theta / M_0$ ) on the circular boundary ( $\theta = -\pi/2$ ) versus the dimensionless central distance of two holes for different wave number under the incident wave with  $\phi_0 = 0$

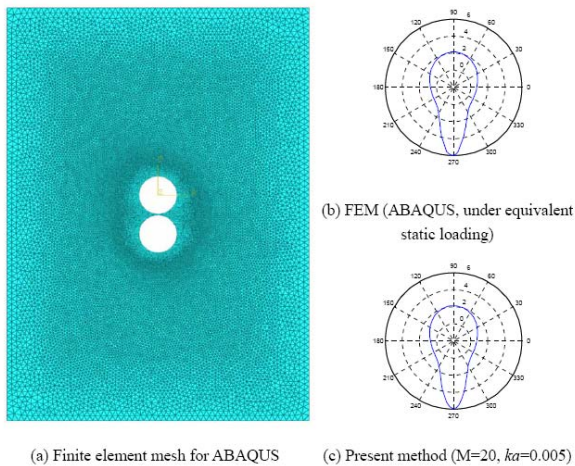


Figure 12 Distribution of DMCF on the upper circular boundary by using different methods, the present method and FEM ( $L/a = 2.1$ )